Fluorescent polymer coated capillaries as optofluidic refractometric sensors

Kristopher J. Rowland,* Alexandre François, Peter Hoffmann, and Tanya M. Monro

The Institute for Photonics and Advanced Sensing, The University of Adelaide Adelaide, South Australia, Australia, 5005

**kristoper.rowland@adelaide.edu.au*

Abstract: A capillary microresonator platform for refractometric sensing is demonstrated by coating the interior of thick-walled silica capillaries with a sub-wavelength layer of high refractive index, dye-doped polymer. No intermediate processing, such as etching or tapering, of the capillary is required. Side illumination and detection of the polymer layer reveals a fluorescence spectrum that is periodically modulated by whispering gallery mode resonances within the layer. Using a Fourier technique to calculate the spectral resonance shifts, the fabricated capillary resonators exhibited refractometric sensitivities up to approximately 30 nm/RIU upon flowing aqueous glucose through them. These sensors could be readily integrated with existing biological and chemical separation platforms such as capillary electrophoresis and gas chromatography where such thick walled capillaries are routinely used with polymer coatings. A review of the modelling required to calculate whispering gallery eigenmodes of such inverted cylindrical resonators is also presented.

OCIS codes: (230.5750) Resonators; (310.6628) Subwavelength structures, nanostructures; (140.3948) Microcavity devices; Microcapillaries; Refractometery; Whispering gallery modes.

References and links

1. I. M. White, H. Oveys, and X. Fan, "Liquid-core optical ring-resonator sensors," Opt. Lett. **31,** 1319–1312 (2006).
2. H. Zhu, I. M. White, J. D. Suter, M. Zourob, and X. Fan, "Integrated refractive index optical ring resonator detector for capillary electrophoresis," Anal. Chem. **79,** 930–937 (2007).
3. S. I. Shopova, I. M. White, Y. Sun, H. Zhu, X. Fan, G. Frye-Mason, A. Thompson, and S. Ja, "On-column micro gas chromatography detection with capillary-based optical ring resonators," Anal. Chem. **80,** 2232–2238 (2008).
4. X. Fan and I. M. White, "Optofluidic microsystems for chemical and biological analysis," Nature Phot. **5,** 591–597 (2011).
5. H. Zhu, I .M. White, J. D. Suter, P. S. Dale, and X. Fan, "Analysis of biomolecule detection with optofluidic ring resonator sensors," Opt. Express **15,** 9139–9146 (2007).
6. G. Yang, I. M. White, and X. Fan, "An opto-fluidic ring resonator biosensor for the detection of organophosphorus pesticides," Sens. Actuators B Chem. **133,** 105–112 (2008).
7. L. Ren, X. Wu, M. Li, X. Zhang, L. Liu, and L. Xu, "Ultrasensitive label-free coupled optofluidic ring laser sensor," Opt. Lett. **37,** 3873–3875 (2012).
8. G. Kemp, "Capillary electrophoresis: a versatile family of analytical techniques," Biotech. Appl. Biochem., **27,** 9–17 (1998).
9. G .Vicente and L. A. Colon, "Separation of bioconjugated quantum dots using capillary electrophoresis," Anal. Chem. **80,** 1988–1994 (2008).
10. J. Horvath and V. Dolník, "Polymer wall coatings for capillary electrophoresis," Electrophoresis **22,** 644–655 (2001).
11. Z. Guo, H. Quan, and S. Pau, "Near-field gap effects on small microcavity whispering-gallery mode resonators," J. Phys. D **39,** 5133 (2006).

#185691 - $15.00 USD Received 26 Feb 2013; revised 7 Apr 2013; accepted 22 Apr 2013; published 3 May 2013

12. C. P. K. Manchee, V. Zamora, J. W. Silverstone, J. G. C. Veinot, and A. Meldrum, "Refractometric sensing with fluorescent-core microcapillaries," Opt. Express **19,** 21540–21551 (2011).
13. A. J. Campillo, J. D. Eversole, and H-B. Lin, "Cavity quantum electrodynamic enhancement of stimulated emission in microdroplets," Phys. Rev. Lett. **67,** 437–440 (1991).
14. A. François and M. Himmelhaus, "Whispering gallery mode biosensor operated in the stimulated emission regime," Appl. Phys. Lett. **94,** 141107 (2009).
15. A. Rose, Z. Zhu, C. F. Madigan, T. M. Swager, and V. Bulovic, "Sensitivity gains in chemosensing by lasing action in organic polymers," Nature **434,** 876–879 (2005).
16. N. Yamasaki, K. Masuyama, A. Fujii, and M. Ozaki, "Spectral modulation of microcapillary laser based on emissive π-conjugated polymers by poor solvent injection," Thin Solid Films **519,** 995–997 (2010).
17. J. R. Rodrguez, J. G. C. Veinot, P. Bianucci, and A. Meldrum, "Whispering gallery modes in hollow cylindrical microcavities containing silicon nanocrystals," Appl. Phys. Lett. **92,** 131119-1–3 (2008).
18. L. Prkna , J. Čtyroký, and M. Hubálek, "Ring microresonator as a photonic structure with complex eigenfrequency," Opt. Quant. Electron. **36,** 259–269 (2004).
19. E. Franchimon, *Modelling Circular Optical Microresonators Using Whispering Gallery Modes*, Thesis (2010).
20. V. Zamora, A. Díez, M. V. Andrés, and B. Gimeno, "Cylindrical optical microcavities: basic properties and sensor applications," Phot. Nano. **9,** 149–158 (2010).
21. K. R. Hiremath, M. Hammer, S. Stoffer, L. Prkna, and Čtyroký, "Analytic approach to dielectric optical bent slab waveguides," Opt. Quant. Electron. **37,** 37–61 (2005).
22. A. W. Snyder and J. Love, *Optical Waveguide Theory* (Springer, 1983).
23. D. R. Rowland and J. D. Love, "Evanescent wave coupling of whispering gallery modes of a dielectric cylinder," Optoelec., IEE Proc. J. **140,** 177–188 (1993).
24. M. Sumetsky, "Mode localization and the Q-factor of a cylindrical microresonator," Opt. Lett. **35,** 2385–2387 (2010).
25. J. W. Silverstone, S. McFarlane, C. P. K. Manchee, and A. Meldrum, "Ultimate resolution for refractometric sensing with whispering gallery mode microcavities," Opt. Express **20,** 8284–8295 (2012).
26. T. Beck, S. Schloer, T. Grossmann, T. Mappes, and H. Kalt, "Flexible coupling of high-Q goblet resonators for formation of tunable photonic molecules," Opt. Express **20,** 22012–22017 (2012).
27. M. Wang, J. Hiltunen, C. Liedert, S. Pearce, M. Charlton, L. Hakalahti, P. Karioja, and R. Myllyl, "Highly sensitive biosensor based on UV imprinted layered polymericinorganic composite waveguides," Opt. Express **20,** 20309–20317 (2012).
28. T. Kobayashi and N. Byrne, "Plastic evanescent microlaser," Appl. Phys. Lett. **99,** 153307-1–3 (2011).
29. J. Huang, V. Bekiari, P. Lianos, and S. Couris, "Study of poly(methyl methacrylate) thin films doped with laser dyes," J Lumin. **81,** 285–291 (1999).
30. S. Atakaramians, K. Cook, H. Ebendorff-Heidepriem, S. Afshar V., J. Canning, D. Abbott, and T. M. Monro, "Cleaving of Extremely Porous Polymer Fibers," IEEE Photon. J. **1,** 286–292 (2009).
31. D. R. Lide (ed.), *CRC Handbook of Chemistry and Physics*, 84$^{\text{th}}$ edition, Chap. 8-66 (CRC Press, 2003).
32. J. Wang and K. Y. Wong, "Polarization characteristics of a light-emitting polymer microring laser," Appl. Phys. B **87,** 685–691 (2007).

1. Introduction

Microresonators have been of recent interest as label-free biological and chemical sensors due to the sensitivity of their resonance spectra to changes in their local environment. Capillary microresonators, such as optofluidic ring resonators (OFRRs) [1], are of particular interest for applications in which they may be integrated with established liquid and gas phase analysis techniques such as capillary electrophoresis (CE) [2] and gas chromatography (GC) [3].

OFRRs are typically silica capillaries whose walls have been reduced in size to a few microns or less via etching and/or tapering methods [1]. Whispering gallery modes (WGMs) are excited in the walls of the capillaries by taper or waveguide coupling. The wavelength-scale size of the thin wall enables the internal evanescent field of the WGMs to overlap with a sample within the capillary, shifting the WGM resonant wavelength as the local environment of the field changes. This allows OFRRs to be used as refractometric sensors in a variety of applications, such as CE [2], GC [3], biosensing [4–6] and ultrasensitive optofluidic sensor designs [7].

Capillary electrophoresis is a versatile liquid- or gel-phase analytical tool that has been employed in a variety of areas ranging from the separation of small molecules to proteins and DNA to chemical cytometry [2, 8]. By loading a capillary with a sample and applying an elec-

#185691 - $15.00 USD Received 26 Feb 2013; revised 7 Apr 2013; accepted 22 Apr 2013; published 3 May 2013

trical voltage to either end, the various mobilities of the species within the sample act to separate them along the length of the capillary [8]. Detection of the separated species typically occurs at the terminal end of the capillary using optical (such as UV absorption or laser induced fluorescence [9]) or other (such as mass spectrometry) techniques to profile the separated species [8]. On-capillary detection is an alternative to end detection that would allow the spatial and temporal profiling of the moving species in-situ, for which OFRRs are a promising candidate [2]. These dynamics are of particular interest for CE modes exhibiting self-focussing, such as the isoelectric focussing (IEF) mode of CE where a neutral inner surface charge prevents the species from globally migrating along the capillary length due to an electro-osmotic flow, instead 'focussing' them to specific points along the capillary. IEF often requires a neutral surface charge, achieved by coating the silica capillaries used with a thin layer of polymer [10].

Gas chromatography is a gas-phase chemical analysis platform that relies on the interaction of the flowed sample's species with a stationary phase and which, as for CE, is often a polymer bound to the internal walls of a silica capillary [3]. Similarly to CE, on-capillary detection is desired in order to resolve the system dynamics and to enable the miniaturisation of the platform towards μGC, where OFRRs are also a promising candidate [3].

However, the thin walls of OFRRs makes them fragile and potentially susceptible to damage or contamination of the outer surface. Waveguide coupling also requires the use of a stable and narrow linewidth laser to scan over the resonance spectrum and stable positioning of the taper [11]. To mitigate such issues, fluorescent core microcapillaries (FCMs) have been demonstrated as an alternative capillary resonator platform by Manchee et al. [12], demonstrating a sensor consisting of a thick walled silica capillary with a high-index inner coating of silicon quantum dots. The emission spectrum of such fluorescent resonators is modulated by the resonance peaks of the WGMs they support due to cavity-QED-enhanced stimulated emission [13]. FCMs thus allow free-space side illumination and detection of the layer's resonances within a robust, thick-walled capillary that does not require etching or tapering and can be handled similarly to the conventional capillaries used in CE and GC. Note that while quantum dots and nanocrystals are desirable for their resistance to photodamage/bleaching [9], they can be non-trivial for certain applications such as inducing lasing, which has been shown to increase the sensitivity and kinetic rate of dye-doped polymer microresonator biosensors [14].

Here, an FCM is demonstrated with a dye-doped high refractive index polymer internal layer, coated using a rapid solvent based deposition method. Capillary microlaser resonators with internal conjugated polymer coatings [15] have been demonstrated [16] and dye-doped polymer microsphere resonators are well established as refractometric sensors, with applications as microlasers and bio-sensors [14]. Polymer coatings are already used extensively in CE [10] and GC [3], making them ideal target platforms for this sensor. It could also find uses as a flow-through sensor from, say, point-of-detection medical diagnostics to industrial process control.

Section 2 describes the modelling and general behaviour of these types of resonators using a complex frequency mode analysis. Section 3 discusses the fabrication method for the internal fluorescent polymer capillary coatings. Section 4 presents the experimental procedure and Fourier analysis (§ 4.1) of the fluorescent resonator refractometric sensing behaviour before a discussion and conclusion is presented in § 5.

2. Inverted cylindrical resonators

Inverted resonators are defined here as those whose exterior refractive index is greater than its interior index, as shown in Fig. 1 (*right*). Thus, in order for practical resonances to be supported, a layer of high refractive index must be introduced between the exterior and interior regions. The higher internal index permits an effective total internal reflection condition, efficiently confining light predominantly within the layer.

#185691 - $15.00 USD Received 26 Feb 2013; revised 7 Apr 2013; accepted 22 Apr 2013; published 3 May 2013

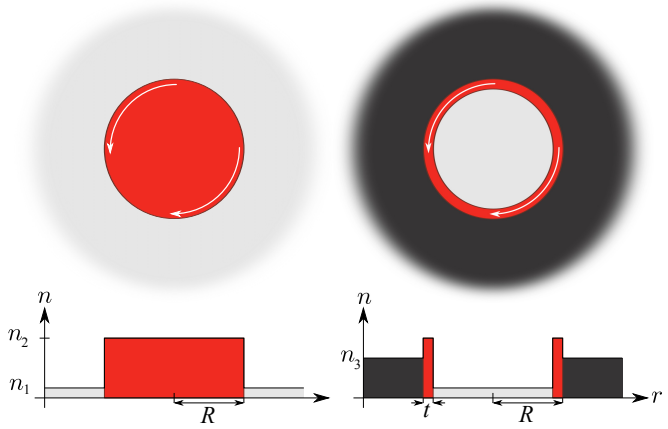

Fig. 1. Schematic diagrams of conventional and inverted cylindrical resonators. Arrows represent the circulation of light about the perimeter of the high index regions (red).

For the thick-walled capillary sensor considered here, the aqueous solution within the capillary has a lower index (n_1) than the silica wall, which has a lower index (n_3) than the internal high-index polymer coating (n_2): $n_2 > n_3 > n_1$. Due to the thick wall, the layer's resonances thus become most sensitive to the *inner channel* of the capillary, rather than the external environment as is the case for most conventional micro-resonator based sensors (Fig. 1, *left*). This allows a flow-through sensor design where the sample being interrogated passes through the resonator itself, as for OFRRs [1] and FCMs [12]. The use of standard thick-walled CE and GC capillaries renders the behaviour of the resonator layer largely immune to changes in the outer environment, while making possible their integration with existing fluidic apparatus.

2.1. Resonances and mode theory

Since inverted resonators are relatively uncommon, and the details of resonator analysis can be subtle, the behaviour and calculation of whispering gallery modes in cylindrical resonators is reviewed here, with a focus on the regime of the fabricated capillary structures described within. A method for calculating the resonant wavelengths of FCMs was discussed by Rodriguez et al. [17] and the method is extended here using a complex frequency eigenvalue technique previously used for multilayer cylindrical [18,19] and thin-walled capillary resonators [20], enabling the calculation of the quality factors (Q) and radiative fields presented below.

All calculations are based on an idealised internally coated capillary with parameters: $n_1 = 1.3329\ldots$ [$n_g(0)$ in Eq. 3 - water], $n_2 = 1.568$ (high-index polymer layer), $n_3 = 1.45$ (silica capillary), capillary radius $R = 25\ \mu$m and various layer thicknesses t. Only transverse electric (TE) modes with an azimuthal order of $l = 350$ (with wavelengths within the spectra of § 4) and radial orders $m = 1$ to 3 are calculated (the only modes with practical Q factors in this regime). TE modes are defined here as those with an electric field component parallel to the cylinder axis [18,19]. The analysis can be applied to arbitrary (multi)layered cylindrical resonators [19].

An approximate resonance condition for a cylindrical resonator (*e.g.*, Fig. 1) can be readily derived. Consider a cylinder of radius R, refractive index n_2 embedded in a homogeneous medium of index n_1. Using a ray approximation, light incident upon the cylinder wall (below the critical angle) will undergo total internal reflection. A *mode* or *resonance* of the cylinder corresponds to light of free-space wavelength λ making one round trip along the resonator perimeter in phase; *i.e.*, the optical path length travelled must be an integer multiple of wavelengths, approximated by $2\pi R = l\lambda/n_2$ where $l \in \mathbb{N}$. The free space wavenumber is $k_0 = 2\pi/\lambda$.

#185691 - $15.00 USD Received 26 Feb 2013; revised 7 Apr 2013; accepted 22 Apr 2013; published 3 May 2013

Light is thus resonant within the cylinder at k_0 values:

$$k_l = l/(n_2 R), \tag{1}$$

or wavelengths $\lambda_l = 2\pi n_2 R/l$, such that the free spectral range (FSR) is $\Delta k = 1/(n_2 R)$ or $\Delta\lambda \approx 2\pi n_2 R/(l^2+l)$, respectively. For the capillary dimensions and materials used here, the FSR can thus be calculated as $\Delta k = 1/(1.568 \times 25\ \mu m) = 0.02551\ldots\ \mu\mathrm{m}^{-1}$; this agrees well with the observed resonance spectra in § 4. Since Eq. 1 only considers the radius of the cylinder and its refractive index, it cannot be used to infer the effects of altering the surrounding index or to describe a capillary (annulus) with changes to its wall thickness or internal index.

To overcome this, a semi-analytic solution to Maxwell's equations is used here to describe the wave nature of the supported resonances. This is important when the resonator surface has a curvature approaching the wavelength scale, allowing light to radiate away from the surface, analogous to a bent waveguide [21]. It also allows the (radiation limited) quality factor Q to be calculated (material loss is not considered here) which is vital when considering sub-wavelength layers; thinner layers increase radiative losses, reducing Q, as shown later.

Electromagnetic fields interacting with cylindrically symmetric structures are readily described by Bessel functions [22, 23]. For a cylindrical resonator, resonances about its circumference can be considered as having an axial wavenumber $\beta = 0$, implying β can't be used as a complex loss term as for leaky waveguides [22]. Instead, the *frequency* ω, or wavenumber $k_0 = \omega/c$, can be considered as complex and treated as the parameter over which to solve the system's characteristic equation $|A| = 0$, where for transverse electric (TE) modes [18, 19]:

$$A(k_0) = \begin{pmatrix} J_l(k_1 r_1) & -J_l(k_2 r_1) & -Y_l(k_2 r_1) & 0 \\ k_1 J_l'(k_1 r_1) & -k_2 J_l'(k_2 r_1) & -k_2 Y_l'(k_2 r_1) & 0 \\ 0 & J_l(k_2 r_2) & Y_l(k_2 r_2) & -H_l^{(1)}(k_3 r_2) \\ 0 & k_2 J_l'(k_2 r_2) & -k_2 Y_l'(k_2 r_2) & -k_3 H_l^{(1)'}(k_3 r_1) \end{pmatrix}, \tag{2}$$

where $r_1 = R - t$, $r_2 = R$, $k_i = k_0 n_i = \omega n_i/c$ and $'$ indicates derivation w.r.t. the argument.

Since the complex frequency is dominant in the oscillatory factor $\exp(-i\omega t)$ of the mode field solutions [18, 22], the imaginary part of $\omega = \omega' + i\omega''$ represents a loss term $\exp(-|\omega''|t)$ (physical solutions for a passive system require $\omega'' < 0$) [18, 19]. The quality factor is thus expressed as $Q = -\omega'/(2\omega'') = -k_0'/(2k_0'')$, where $k_0 = k_0' + ik_0''$ [18, 20].

Even though skew rays exist in practice ($\beta > 0$), high Q azimuthal resonances still dominate [24]. Indeed, the resonance spectra measured here (shown later in Fig. 6) exhibit peaks skewed to short λ, a result of cylindrical resonator skew rays [12, 25]. Nonetheless, as shown in § 4, the $\beta = 0$ resonances from Eq. 2 match well with the measured behaviour.

$|A| = 0$ was solved numerically via the Python scripting language with the *SciPy* and *matplotlib* libraries. Each solution takes a few seconds to solve (2.5 GHz, Intel® Core™ i5 CPU) using a linear bisection method where $|A|$ is minimised along linear slices taken along the ω'' axis, with consecutive slices taken closer to the solution pole, alternating in the imaginary then real dimensions, until a threshold minimum is reached. When this failed to find a pole, an exhaustive search of the complex plane was employed (a slower method).

The system is sensitive to the resonator parameters, so an accurate ω guess value must be used in the minimisation [19]. Here, Eq. 1 is successfully used as a guess in all calculations presented, typically within about 10% of ω' of the fundamental $m = 1$ solution, readily allowing all modes to be tracked as resonator parameters are varied as in Tab. 1 and Fig. 2.

The mode fields shown in Fig. 2 are evaluated by calculating the kernel K of A at a given k_0, where $K = (A, B, C, D)$ such that $AK = 0$, via a singular value decomposition method [NumPy's `svd()` function]. The fields are then evaluated as $\psi(r) = AJ_l(k_1 r),\ BJ_l(k_1 r) + CY_l(k_2 r)$ or $DH_l^{(1)}(k_3 r)$ for $r \le r1$, $r_1 < r \le r2$ or $r \ge r2$, respectively (light grey, red and dark grey regions

#185691 - $15.00 USD Received 26 Feb 2013; revised 7 Apr 2013; accepted 22 Apr 2013; published 3 May 2013

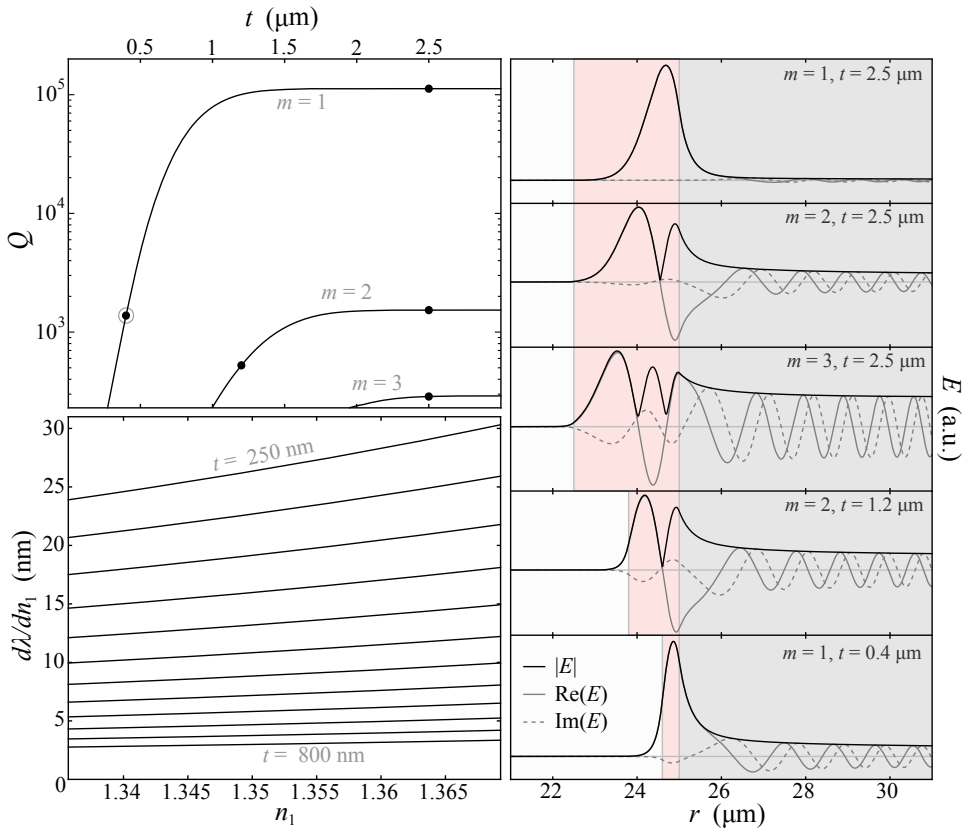

Fig. 2. Properties of the whispering gallery modes within the high-index layer of the capillary resonator vs. layer thickness t for azimuthal order $l = 350$. *Top left:* Q of the modes with radial orders $m = 1$, 2 and 3 over a range of t for $n_0 = n_g(0) = 1.3329\ldots$ (water, see Eq. 3). *Right:* The modes' electric field for the layer thicknesses indicated by the solid black points on the Q plot, each normalised to the maximum value of $|E|$. Their associated mode properties are listed in Tab. 1. The capillary sensors demonstrated in §§ 3 and 4 have layer thicknesses close to the calculated $t = 400$ nm $m = 1$ mode (circled dot and bottom field profile). *Bottom left:* Sensitivity of the $m = 1$ resonance wavelength to changes in the inner channel index n_1 for $t = 250$ nm $\rightarrow$ 800 nm in steps of 50 nm.

Table 1. Summary of the properties (rounded to 6 significant figures) of the modes whose fields are shown above (Fig. 2, *right*) and are represented by the solid black points in the $Q(t)$ plot (Fig. 2, *top left*). All have azimuthal mode order $l = 350$.

t (μm)	m	ω ($\times 10^{10}$ rad/s)	λ (nm)	Q
2.5	1	275544 - 1.22562i	683.611	112410
2.5	2	282911 - 92.3465i	665.811	1531.79
2.5	3	289103 - 504.484i	651.551	286.533
1.2	2	284580 - 271.190i	661.904	524.688
0.4	1	280858 - 101.955i	670.678	1377.36

#185691 - $15.00 USD Received 26 Feb 2013; revised 7 Apr 2013; accepted 22 Apr 2013; published 3 May 2013

in Fig. 2), where for TE solutions ψ is the electric field E and is polarized along the capillary axis [18,19]. The Hankel function expression for the outer fields implies all solutions outwardly radiate with an oscillating external field; the magnitude of the radiation loss is captured by the imaginary part of ω (hence Q), analogous to a bent waveguide [21].

Each solution has azimuthal and radial mode orders l and m respectively. l is a free parameter of A (Eq. 2) and related to mode fields with l azimuthal nodes due to their $\exp(il\theta)$ angular (θ) dependence [18,19]. The m^{th} solutions in the direction of the ω' axis produce m radial intensity maxima (see Fig. 2), related to m being in the radially dependent field arguments [22].

2.2. Effective single-modedness

Figure 2 demonstrates some of the mode properties unique to the inverted capillary resonator, in particular the influence of the high-index layer thickness t. For large t, the resonator behaves as a solid cylinder since the field decays substantially before reaching the inner layer interface; the modes' Q thus plateaus for increasing t. Since $n_3 > n_1$, light readily radiates into the higher index as t decreases. Since resonances can only efficiently exist in the high-index layer, this produces an effective single-moded behaviour: as t decreases, the inner layer interface encroaches on the inner tails of the mode fields, 'pushing' them to the outer interface, increasing the amplitude of the outer radiative field components (Fig. 2) and decreasing the Q. Since the field of the fundamental $m = 1$ resonance decays faster as $r \to 0$ than the $m > 1$ resonances, and higher order capillary modes typically have a lower Q [20], the $m = 1$ mode maintains a larger Q for thinner layers. Similar effects have been described for thin-walled capillaries [20].

Resonance peaks are readily discernible if their (FWHM) width δk is narrower than their FSR Δk [25]. For a measured $Q_{\text{meas.}} = k_0/\delta k$ [12, 14], and assuming a maximum detectable peak width of half the FSR $\delta k \leq \Delta k/2$, the capillary parameters here imply practical Q factors of $Q \geq k_0 n_2 R \approx 370$ (for $\lambda \approx 660$ nm – Tab. 1 and Fig. 6). Thus, from Fig. 2 (*top-left*), the capillary here should be effectively single moded for layer thicknesses $t \lessapprox 1.1\ \mu$m.

As shown in § 3, these layer dimensions are readily fabricable. Supporting a single radial whispering gallery mode is ideal for producing clean fluorescence spectra combs, since the homogeneous distribution of dye within the layer excites all available modes. Such clean resonance combs are ideal for measuring the sensitivity of the device using Fourier techniques to extract small spectral shifts [25], as used in § 4.1.

Figure 2 also shows how the sensitivity increases for larger n_1, especially for smaller t. This is explained by the fact that a higher internal index will 'pull' the field toward it, thereby increasing the field overlap with the interior region and thus the modes' sensitivity to changes in n_1. This effect is increased for thinner layers since the internal evanescent field is already enhanced in this region, as per the field profiles of Fig. 2.

3. Fabrication

A solvent evaporation deposition method was devised for the internal coating of silica capillaries with a 50 μm inner diameter and $\approx 360\ \mu$m outer diameter (Polymicro). Where the internal coating of a capillary differs to spin coating, say, is the conformation of the surface: the interior surface of a capillary is concave. The capillary forces of a loaded solution can be used to allow the deposition of even polymer layers within a capillary [16] and is the principle exploited here.

The method employed here involves dissolving a polymer within a suitable solvent, filling a section of capillary with the solution and heating the capillary at a given temperature. As the solvent evaporates from the solution within the capillary, the meniscus of the fluid leaves behind a thin layer of polymer on the surface as it retreats down the length of the capillary. Since the concentration of polymer to solvent of the fluid increases as the solvent evaporates, a solid plug of polymer typically remains at one end of the capillary after baking; this end

#185691 - $15.00 USD Received 26 Feb 2013; revised 7 Apr 2013; accepted 22 Apr 2013; published 3 May 2013

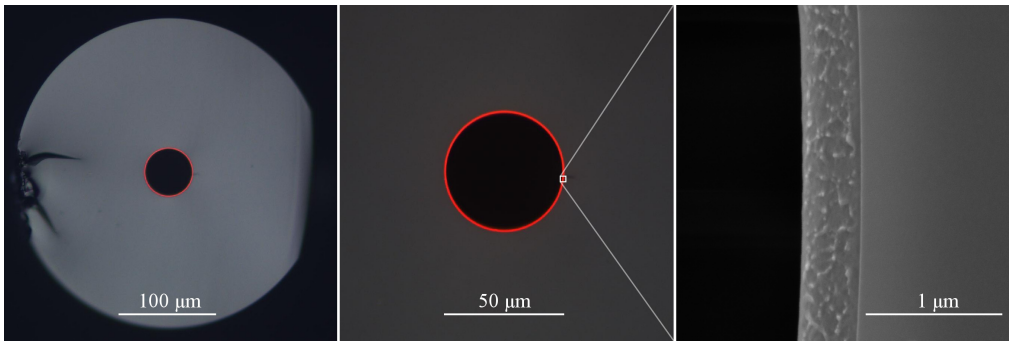

Fig. 3. *Top* and *center*: optical micrographs of a cleaved end of a capillary internally coated with Nile Red doped PB_ZMA. Note the uniform thickness of the coating (fluorescent red ring). *Right*: scanning electron micrograph (SEM) of a section (white square in the *center* image) of a polymer layer.

was cleaved off to allow unimpeded flow through the capillary length. While this increase in polymer concentration could lead to a gradient in layer thickness along the capillary, it has not been characterised here and was obvious only within about 1 cm of solid plug (and discarded).

Here the polymer poly(benzyl methacrylate) (PB_ZMA, PolySciences) was used since it has a refractive index (1.568) significantly higher than that of silica ($\Delta n \approx 0.118$) and otherwise similar properties to the more common poly(methyl methacrylate) (PMMA) often used in optical devices [26, 27] including cylindrical microlasers [28]. It was also anticipated that PB_ZMA could be readily doped with laser dyes as for PMMA [28, 29], and is demonstrated here.

The solvent was chosen so that its boiling point was comparable to the transition temperature of the polymer ($T_g \approx 54\ ^\circ C$), in order to avoid the polymer melting at the temperatures used to evaporate the solvent, but not so low as to readily evaporate at room temperature, allowing convenient handling. The solvent must also be able to dissolve the polymer adequately, forming a homogeneous solution. Here, Tetrahydrofuran (THF) was found to be suitable. The boiling point of THF is $\approx 66\ ^\circ C$ and produced a clear, homogeneous solution of dissolved PB_ZMA after mixing in a glass vial and leaving for 48 hours. For these trials, small volumes of the mixture were prepared at a concentration of 50 mg/mL polymer to solvent.

A preparation of fluorescent dye was added to the dissolved polymer solution: Nile Red (Sigma Aldritch) dissolved within THF. A saturated solution was prepared by adding and mixing the dye powder into the solvent until it could no longer be dissolved. The solution was left for a few days prior to use, allowing the undissolved dye particles to settle. 10 μL of this saturated solution was added to 200 μL of the polymer solution and thoroughly mixed.

Since the capillaries come with a thick external protective polyimide coating (brown in colour – not ideal for visible light transmission), a section of this coating was removed via a flame to form an observation window, then the outside surface was cleaned with acetone.

The dye-doped polymer solution was manually loaded into 10 cm lengths of these prepared capillaries by piercing a capillary through the rubber septum of a capped glass vial containing the doped polymer solution, ensuring the end of the capillary was immersed in the solution. The vial was then internally pressurised, using an air filled syringe pierced through the septum, until the solution traversed just beyond the far side of the capillary window. These loaded capillaries were placed horizontally into an oven at 75°C and left for about 15 minutes.

Figure 3 shows micrographs of a coated capillary, cleaved after the oven baking step. The coating was symmetric to within $\approx$ 2.5 % of the inner diameter with average thickness $\approx$ 400 nm. The polymer layer cleave conforms to the silica cleave due to the layer being so

#185691 - $15.00 USD Received 26 Feb 2013; revised 7 Apr 2013; accepted 22 Apr 2013; published 3 May 2013

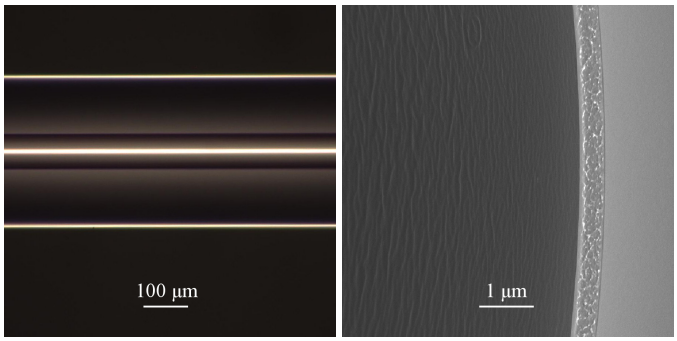

Fig. 4. *Left*: optical micrograph side view of a Nile Red doped PB_ZMA internally coated capillary (windowed section where the protective outer coating has been removed). *Right*: scanning electron micrograph of a cleaved end of a prepared capillary (same sample as Fig. 3), revealing the inner surface of the layer by tilting the sample.

thin and adhesion of the polymer to the silica. An uneven surface was observed on the cleaved polymer surface, as may be expected since polymers are notoriously difficult to cleave due to their long molecular chains [30], but is of little consequence here. Figure 4 shows that the inner surface of the layer was comparably very smooth but with longitudinal waves observed, likely due to nature of deposition process, but which do not appear to significantly affect the resonances of the layer. With this fabrication routine, a coating was successfully deposited each time, up to the thickness variations discussed below.

4. Experiment

The sensitivity of the capillary resonators to the refractive index of the solution flowed through them was determined by measuring the relative shift of the resonance peaks of the polymer layers' fluorescence spectra using the apparatus of Fig. 5.

Mixtures of glucose (Sigma Aldrich) and water of increasing refractive index were flowed

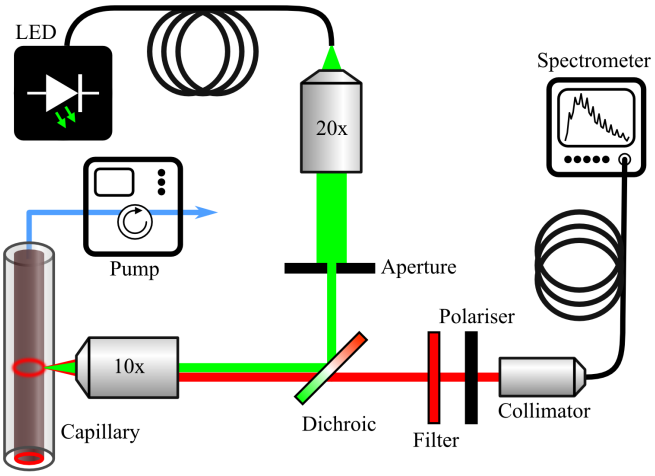

Fig. 5. A schematic of the apparatus used to flow solutions through a coated capillary and detect the WGM modulated fluorescence spectrum of the dye doped polymer layer.

#185691 - $15.00 USD Received 26 Feb 2013; revised 7 Apr 2013; accepted 22 Apr 2013; published 3 May 2013

through each capillary using a peristaltic pump. Five solutions were prepared with glucose to water concentrations of: pure (millipore) water, 6.2573 g/dL, 12.515 g/dL, 18.772 g/dL and 25.029 g/dL. These concentrations correspond to refractive indices of approximately 1.3329, 1.3427, 1.3525, 1.3623 and 1.3721, calculated here by fitting a linear interpolant to the refractive index vs. glucose weight to water volume concentration values 0.5 g/dL ($n_g = 1.3736$) and 26 g/dL ($n_g = 1.3736$) listed in Ref. [31], producing:

$$n_g(C) = 1.564705\ldots \times 10^{-3} C + 1.332917\ldots \tag{3}$$

where n_g and C are the refractive index and concentration (g/dL) of the solution.

For each coated capillary, approximately 1 cm of one end was inserted into the tubing (Ismatech Tygon 380 μm inner diameter) of a peristaltic pump (Longerpump BT100-1F, 10 roller head). The other end of the capillary was inserted into a ≈ 10 cm length of the same peristaltic tubing; this tubing was immersed into the solutions of interest, reducing the dead volume of fluid flow prior to the capillary. Prior to use, the prepared capillaries were flushed with water for 18 hours in order to condition them by removing excess solvent and allowing the water to fill any surface defects; it is anticipated that refined fabrication could mitigate this step.

The prepared capillary was mounted transversely upon an alignment stage (Thorlabs, 3-Axis NanoMax), allowing alignment of a microscope objective with respect to the side of the capillary. The fluorescent polymer layer was illuminated from the side through the window of the capillary. An green LED source (Thorlabs, 530 nm, 5.1 mW) was used, coupled to a large core (1 mm) patch cable and collimated. A dichroic mirror (532 nm long pass transmission) was used to reflect the pump light through the objective on the stage and excite the dye. The fluorescent emission from the layer was then recaptured back through the same objective and transmitted through the dichroic mirror, passed through a linear polarizer and coupled into a spectrometer (Horiba Jobin Yvon iHR320, 600 line grating) via a 400 μm patch cable (collimated onto the spectrometer slit). The linear polarizer was used to sample only the TE polarized resonances. Note that TM resonances with somewhat lower visibility were also observed by rotating the polarizer by 90°, similarly to Ref. [12], but are not reported here due to their qualitatively similar behavior to the TE resonances.

The target solutions were flowed through the capillary for at least 15 minutes prior to each illumination to ensure stability. The flow rate at all times was 5 μL/min, but was stopped when changing samples. Three capillaries were tested, fabricated in the same batch. For each, the optical alignment was optimised to maximise the fluorescence peak visibility.

After optimising the alignment of the fluorescence excitation and collection optics, sharp resonance peaks were observed in the fluorescent layer's emission spectrum, as shown in Fig. 6. By measuring the spectral width of the peaks, the measured quality factor was $Q_{\text{meas.}} \approx 800$, which is within the range predicted for the $m = 1$ mode for similar t in § 2, Fig. 2 (*top left*).

4.1. Analysis

Calculation of the wavelength shift of the spectra was based on a Fourier technique described by Silverstone et al. [25]: the Fourier transform of the spectra $F(\nu) = \mathscr{F}\{I(k)\}$ (ν is the Fourier frequency) is calculated and the Fourier phase of the major frequency peak is found. Changes in the value of the phase correspond to spectral shifts of the modulated fluorescence comb. It has been shown [25] that, for fluorescent capillary resonators, this method is superior to either peak picking or peak fitting in which the shift of a single peak is tracked rather than the shift of all peaks as a whole. Further, this Fourier technique requires resolution mainly of low frequency Fourier components – related to the FSR of the resonator (c.f. Eq. 1) – rather than the high frequency components required to identify sharp spectral peaks. Thus, to decrease detection limits, sharp resonance peaks due to large Q factors are not critical here; it is more important to improve the signal to noise ratio to better define the low frequency Fourier terms [12, 25].

#185691 - $15.00 USD Received 26 Feb 2013; revised 7 Apr 2013; accepted 22 Apr 2013; published 3 May 2013

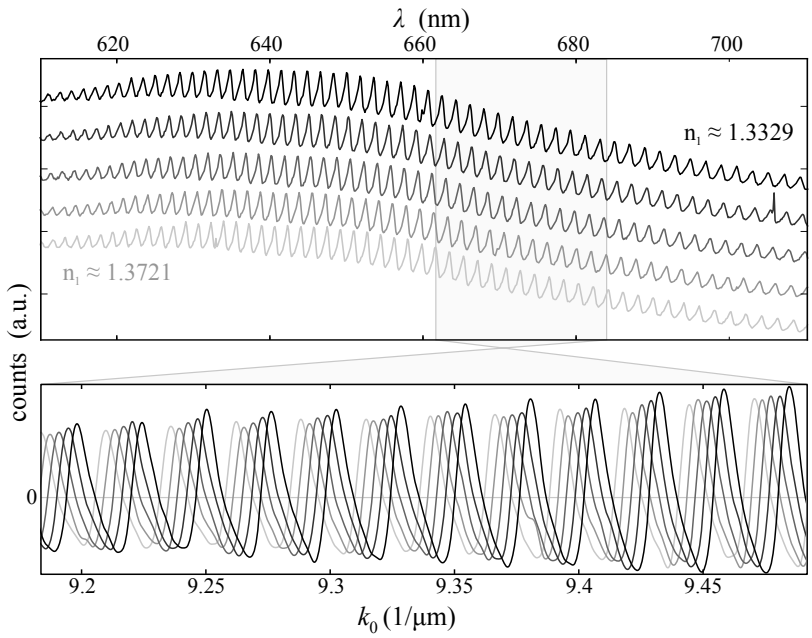

Fig. 6. *Top*: fluorescence spectra of an internal dye doped polymer layer (capillary C1, Fig. 7) following flushing of the capillary with the target solutions, increasing n_1 from top to bottom – vertically offset for clarity. *Bottom*: the same spectra (overlayed) with a wide (10% full spectral window) moving average subtracted and converted to k_0 space for analysis (as per § 4.1).

A broad moving average (10% of the spectral window) was applied to, then subtracted from, each spectrum, thus removing the fluorescence background, leaving the resonance peaks. A Hanning function was applied to the spectra before Fourier analysis to reduce edge artefacts.

Since the FSR should be equal for all peaks over k_0 as per Eq. 1, relating to a single Fourier component along the k_0 axis, the fluorescence spectra are converted from wavelength to wavenumber space via linear interpolation [25]. The major Fourier frequency peak of all spectra considered here (*e.g.*, Fig. 6) was thus very sharp, constituting a single point $F(\nu^{'}) = F^{'}$ in the real part of the complex Fourier spectrum $F(\nu)$. The phase of the complex F', $\phi^{'} = \arg(F')$, was calculated and used to derive the wavenumber shift via $\Delta k = \phi^{'}/(2\pi\nu^{'})$. This shift is relative to the same (arbitrary) wavenumber limits of each spectrum, allowing consecutive shifts to be compared. Note also that the periodicity of the phase must be taken into account where $\phi^{'}$ can change sign while traversing a FSR; these jumps are accounted for in the data analysis.

The shifted wavelength $\lambda^{'}$ here was calculated relative an arbitrary reference wavelength ($\overline{\lambda} = 600$ nm and $\overline{k} = 2\pi/\overline{\lambda}$) via $\lambda^{'} = 2\pi/k^{'} = 2\pi/(\overline{k} - \Delta k)$. For small Δk, the standard approximate bandwidth conversion can also be used: $\Delta\lambda \approx \Delta k\overline{\lambda}^2/2\pi$. Note that $\overline{k}$ (and $k^{'}$) is not required to calculate Δk as above and hence is equal across all wavenumbers; however, the choice of $\overline{\lambda}$ does affect the value of $\Delta\lambda$ and was arbitrarily chosen here to be close to the short wavelength end of the fluorescence spectrum. For such wide-band spectra as from FCMs, their sensitivities are thus better described by shifts in the wavenumber (or frequency) space, as per Δk, but $\Delta\lambda$ is used here as it is common in the literature. $\Delta\lambda$ in Fig. 7 was calculated as a shift from the first (water) sample, $\Delta\lambda = \lambda^{'} - \lambda^{'}|_{\text{water}}$, such that the first value is always $\Delta\lambda = 0$.

$\Delta\lambda$ for all glucose solutions flowed through each of the three capillaries is shown in Fig. 7,

#185691 - $15.00 USD Received 26 Feb 2013; revised 7 Apr 2013; accepted 22 Apr 2013; published 3 May 2013

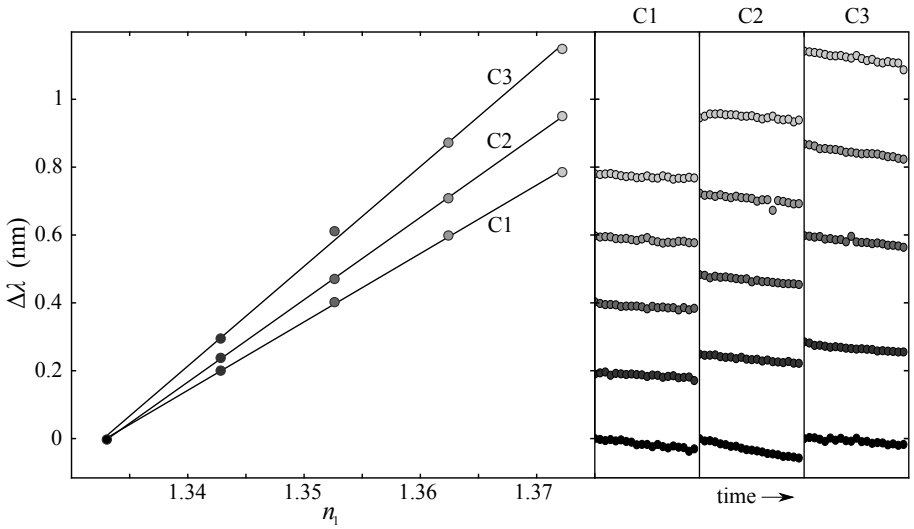

Fig. 7. *Left*: wavelength shifts of three coated capillaries upon flushing with glucose solutions of increasing concentration (refractive index). Data points represent the Fourier-derived shift of the time-averaged spectra. Lines represent a linear fit to each series of shifts. *Right*: time series of $\Delta\lambda$ for each capillary, each spanning 10 minutes with equal time steps. For this figure, a reference wavelength of $\overline{\lambda} = 600$ nm was used for all calculations of $\Delta\lambda$.

where a linear fit has been made for each capillary. The fits' slopes correspond to the sensitivity of capillaries C1, C2 and C3 to changes in the flowed solution's refractive index: 20.2 nm/RIU, 24.3 nm/RIU and 29.4 nm/RIU, respectively. The wavenumber sensitivities were $3.52 \times 10^{-4}/(\text{nm RIU})$, $4.24 \times 10^{-4}/(\text{nm RIU})$ and $5.13 \times 10^{-4}/(\text{nm RIU})$ and are independent of a reference, as discussed. (At a longer reference wavelength $\overline{\lambda} = 660$ nm, in the middle of the fluorescence spectrum, the wavelength sensitivities increase to 24.4 nm/RIU, 29.4 nm/RIU and 35.6 nm/RIU.) These values correspond well to the semi-analytic model calculations of § 2 where, assuming the validity of the refractive indices used, the sensitivities correspond to layer thicknesses of approximately 376 nm, 324 nm and 267 nm, respectively, which is comparable to the measured layer thickness of the sample shown in Fig. 3. Such variations in thickness are expected from this first demonstration of the fabrication method proposed in § 3 and are expected to be minimised with refined techniques.

The analyzed spectra (*e.g.*, Fig. 6) were actually averages of time series, shown in Fig. 7: for each solution, 20 acquisitions were made for 2 seconds each at equal intervals over 10 minutes. By also applying the Fourier analysis to each spectrum of the time series, the resonance shifts for each exposure could be tracked. Figure 7 reveals that there was a small but consistent drift in the resonance wavelength. By applying a linear fit to each set of 20 acquisitions, the drift was calculated to be about -30 pm/sample. The source of this drift could be leaching of residual solvent in the polymer into the aqueous samples (THF is miscible with water).

This drift was observed to be much larger (in the same direction and with an exponential decaying trend) when the 18 hour pre-flushing step was omitted. Assuming this drift approximates the measurement uncertainty in the spectral shift for a given sample, and assuming a sensitivity of 30 nm/RIU, the minimum detection limit would be 10^{-3} RIU, which is lower than the spectrometer-limited precision quoted for the nanocrystal coated capillary sensor of Manchee et al. [12]. However, the time series also shows rapid but small fluctuations in the measured resonance shifts with a standard deviation of about 3 pm about the drift trend. If the

#185691 - $15.00 USD Received 26 Feb 2013; revised 7 Apr 2013; accepted 22 Apr 2013; published 3 May 2013

drift could be eliminated through refined fabrication and experimentation, this would imply a minimum detection limit of about 10^{-4} RIU for the same sensitivity. It is expected that with the use of polymers with higher refractive indices, the deposition of thinner layers (*e.g.* the calculations of Ref. [12]) and refinement of the fabrication and experimental method, this detection limit could be substantially reduced even further.

5. Discussion and conclusion

The above results demonstrate the fabrication of a flow-through capillary microresonator sensor made from a standard thick walled silica capillary, as used in CE or GC, by coating its interior wall with a thin film of dye-doped PB_ZMA at thicknesses of approximately 250 nm to 400 nm. Sensitivities up to approximately 30 nm/RIU were demonstrated by flowing through glucose solutions. A Fourier phase analysis method was employed to efficiently and accurately resolve the shifts of the WGM resonance modulated fluorescence spectral comb. The results agreed well with simulations based on a complex frequency eigenvalue model.

The motivation for this work was the creation of a label-free sensor that could be readily integrated with (bio)chemical separation platforms such as CE and GC; platforms where internally polymer coated capillaries are routinely employed. The use of robust industry standard capillaries with an internal coating of high index fluorescent polymer could allow the sensor to be connected in-line with existing capillary systems (via readily available fluidic connectors and ferrules), or to replace the capillaries entirely, without damaging the resonator layer itself. Transverse excitation and detection of the resonator's fluorescence makes such enhancements to existing capillary systems minimally invasive, avoids the requirement of waveguide coupling and offers the potential of resolving longitudinal variations along the capillary in both space and time. Indeed, they could also be used as integral components in miniaturised CE and μGC [3] platforms for optofluidic lab-on-a-chip applications.

The use of an inner polymer coating makes these sensors ideal for applications to capillary electrophoresis: in isoelectric focussing mode, silica capillaries with an internal polymer coating are often employed in order to suppress the effects of the electro-osmotic flow otherwise induced by the surface charges of the inner surface [10], where care must be taken for the thin layer (often a few nm) not to degrade. This thicker layer could provide a neutral surface and be more resistant to degradation. Further, on-capillary detection using capillary resonators could allow the complex dynamics of the focussing species to be tracked in-situ, while leveraging the benefits of a sensitive and label free WGM sensing mechanism [2].

Similarly, gas chromatography routinely uses internal polymer coatings as a stationary phase for the separation of gaseous species. Thin-walled glass capillaries coated with an internal polymer stationary phase have recently been demonstrated [3]. By confining light inside the polymer layer itself, as was demonstrated here, rather than predominantly in a thin glass wall, the sensitivity of these systems could be substantially increased.

The simple and quick solvent based low-temperature coating method outlined in § 3 is versatile in that a wide range of polymers and dyes could potentially be used to coat the capillary interior. Indeed, this platform may point a way towards the use of light emitting organic and conjugated polymers for gas flow and optofluidic microlaser sensors [15, 16] for biological and chemical targets. The capillary, polymer, solvent, oven and LED light source used here are readily available and cheap in comparison to the resources required for alternative microresonator sensor designs; the spectrometer remains the most expensive component, although more cost effective units tailored to the application could be used. Simple and rapid fabrication methods and cost scalability are important aspects to sensor designs with the potential for integration or multiplexing with existing platforms such as CE and GC or as a sensor in and of itself as, say, a portable, point-of-care diagnostic apparatus.

#185691 - $15.00 USD Received 26 Feb 2013; revised 7 Apr 2013; accepted 22 Apr 2013; published 3 May 2013

Acknowledgments

This research was supported under an Australian Research Council *Super Science Fellowship* (project number FS100100039). The authors would like to acknowledge Dr Shahraam Afshar V. and Dr Matthew Henderson for enlightening discussions regarding the behaviour and theoretical analysis of cylindrical resonators. Dr Georgios Tsiminis is gratefully acknowledged for illuminating discussions related to light emitting polymers and microlasers.

#185691 - $15.00 USD Received 26 Feb 2013; revised 7 Apr 2013; accepted 22 Apr 2013; published 3 May 2013